PERK Inhibition by HC-5404 Sensitizes Renal Cell Carcinoma Tumor Models to Antiangiogenic Tyrosine Kinase Inhibitors

Michael E. Stokes[1], Veronica Calvo[1], Sho Fujisawa[1], Crissy Dudgeon[1], Sharon Huang[1], Nupur Ballal[1], Leyi Shen[1], Jennifer Gasparek[2], Matthew Betzenhauser[2], Simon J. Taylor[3], Kirk A. Staschke[4,5], Alan C. Rigby[1], Mark J. Mulvihill[1], Nandita Bose[1], Eric S. Lightcap[1], and David Surguladze[1]

ABSTRACT

Purpose: Tumors activate protein kinase R (PKR)-like endoplasmic reticulum kinase (PERK, also called EIF2AK3) in response to hypoxia and nutrient deprivation as a stress-mitigation strategy. Here, we tested the hypothesis that inhibiting PERK with HC-5404 enhances the antitumor efficacy of standard-of-care VEGF receptor tyrosine kinase inhibitors (VEGFR-TKI).

Experimental Design: HC-5404 was characterized as a potent and selective PERK inhibitor, with favorable *in vivo* properties. Multiple renal cell carcinoma (RCC) tumor models were then cotreated with both HC-5404 and VEGFR-TKI *in vivo*, measuring tumor volume across time and evaluating tumor response by protein analysis and IHC.

Results: VEGFR-TKI including axitinib, cabozantinib, lenvatinib, and sunitinib induce PERK activation in 786-O RCC xenografts. Cotreatment with HC-5404 inhibited PERK in tumors and significantly increased antitumor effects of VEGFR-TKI across multiple RCC models, resulting in tumor stasis or regression. Analysis of tumor sections revealed that HC-5404 enhanced the antiangiogenic effects of axitinib and lenvatinib by inhibiting both new vasculature and mature tumor blood vessels. Xenografts that progress on axitinib monotherapy remain sensitive to the combination treatment, resulting in ∼20% tumor regression in the combination group. When tested across a panel of 18 RCC patient-derived xenograft (PDX) models, the combination induced greater antitumor effects relative to monotherapies. In this single animal study, nine out of 18 models responded with ≥50% tumor regression from baseline in the combination group.

Conclusions: By disrupting an adaptive stress response evoked by VEGFR-TKI, HC-5404 presents a clinical opportunity to improve the antitumor effects of well-established standard-of-care therapies in RCC.

Introduction

Antiangiogenic agents form the backbone of standard of care for advanced renal cell carcinoma (RCC), but their clinical impact is limited by primary and secondary resistance mechanisms that remain a critical problem (1, 2). Multitargeted tyrosine kinase inhibitors that block VEGFR (VEGFR-TKI) have had success in RCC, leading to initial approvals of sunitinib and sorafenib as first-line therapies in 2005 and 2006, respectively (3, 4). Since then, second-generation VEGFR-TKI have been developed and approved in advanced RCC, including axitinib (5, 6), lenvatinib (7, 8), cabozantinib (9, 10), and tivozanib (11), among others. These second-generation VEGFR-TKI have improved selectivity and efficacy over sorafenib and sunitinib, but for most patients, their benefits are short-lived as tumors develop evasive strategies to overcome the effects of VEGFR-TKI (2). Throughout the course of therapy, a patient may be sequentially treated with multiple VEGFR-TKI as tumors develop resistance to specific agents, resulting in multiple lines of therapy centered around the VEGF/-VEGFR axis (12, 13).

By disrupting tumor vascular development, antiangiogenic VEGFR-TKI promote hypoxia and nutrient deprivation that drives endoplasmic reticulum (ER) stress (10, 14). Tumors can evade deleterious ER stress through activation of the PERK branch of the integrated stress response (ISR; refs. 15, 16). Under hypoxic conditions, the accumulation of misfolded proteins in the ER lumen results in the dimerization and transautophosphorylation of PERK, which subsequently phosphorylates eIF2α(Ser51) to attenuate global protein synthesis while enabling selective translation of proteins that restore homeostasis (17). One such factor is ATF4, a transcription factor that drives the expression of genes involved in antioxidant response and amino acid metabolism and transport, which are meant to promote cell survival during bouts of intermittent ER stress (15, 17, 18). Thus, PERK activation supports tumor cell survival by mitigating the inhibitory effects of hypoxia through the decreased rates of protein synthesis that alleviate ER stress.

In addition to mitigating stress, PERK directly supports vascular development in response to hypoxia or nutrient deprivation (19, 20). *In vitro*, the induction of ER stress by glucose deprivation results in PERK-dependent expression and secretion of the proangiogenic factors VEGF, FGF-2, and IL6, which are sufficient to induce vascular sprouting in endothelial cells (19). *In vivo*, knocking down PERK using short-hairpin RNAs in the squamous carcinoma head and neck model UM-SCC-74B significantly inhibited tumor volume and resulted in tumors with decreased blood vessel density (19). PERK is also involved in vascular responses to antiangiogenics: prolonged sunitinib

[1]HiberCell, Inc., New York City, New York. [2]Curia, Buffalo, New York. [3]Drug Discovery, Pharmaron UK Ltd., Hoddesdon, Herts, United Kingdom. [4]Indiana University School of Medicine, Indianapolis, Indiana. [5]Indiana University Melvin and Bren Simon Comprehensive Cancer Center, Indianapolis, Indiana.

M.E. Stokes and V. Calvo contributed equally to this article.

Corresponding Author: Michael E. Stokes, HiberCell, Inc., 619 West 54th Street, New York City, NY 10019. E-mail: mstokes@hibercell.com

Clin Cancer Res 2023;29:4870–82

doi: 10.1158/1078-0432.CCR-23-1182

Translational Relevance

The PERK inhibitor HC-5404 is currently undergoing first-in-human clinical evaluation for safety and tolerability in a phase I solid tumor clinical trial. The studies presented herein support a rationale for combining HC-5404 with standard-of-care VEGFR-TKI in patients with RCC. HC-5404 enhanced sensitivity to all VEGFR-TKI tested across a diverse collection of RCC tumor models and demonstrated vascular effects distinct from those achieved with VEGFR-TKI alone, highlighting multiple clinical opportunities to improve patient outcomes. RCC tumors often develop resistance to VEGFR-TKI, limiting their clinical utility and necessitating new combination partners that inhibit the adaptive pathways tumors use to overcome targeted therapies. As xenografts that progress on axitinib remain sensitive to the combination treatment, it is likely that HC-5404 can also benefit patients in the second- and third-line settings. This novel therapeutic combination is an opportunity to improve patient outcome in RCC and in additional indications for which VEGFR-TKI are approved.

treatment drove PERK-dependent induction of proangiogenic cytokines that supported secondary resistance to sunitinib (21). These studies highlight a possible role for PERK in promoting angiogenic cues that drive vascular development in response to hypoxia and ER stress.

HC-5404 is a potent and selective PERK inhibitor currently in first-in-human phase I clinical trials (NCT04834778). Here, we test the hypothesis that PERK inhibition increases tumor response to antiangiogenic agents using HC-5404. We found that combining HC-5404 with multiple VEGFR-TKI provided a combination benefit that enhanced the effects of each VEGFR-TKI, driving tumor regression across diverse tumor models of RCC. HC-5404 enhanced the antiangiogenic effects of VEGFR-TKI, highlighting the role that PERK plays in protecting vascular cells from antiangiogenic agents. Together, these findings provide a clinical rationale for combining PERK inhibitors with antiangiogenic therapies in RCC.

Materials and Methods

Chemistry

HC-5404 was synthesized and validated according to previously established protocols (22).

Biochemical assays

The potency of HC-5404 against four ISR kinases was evaluated in cell-free FRET-based biochemical assays, the methods of which are described elsewhere (22, 23). Kinome specificity was evaluated using a KINOMEScan biochemical panel assay (Eurofins Discovery; ref. 24).

Cell-based studies

HEK-293 cells (ATCC, CRL-1573; RRID:CVCL_0045) were plated at 1×10^6 cells per well and pretreated with various doses of HC-5404 30 minutes prior to addition of 1 μmol/L tunicamycin (Sigma, T7765) to induce ER stress. After 4 hours, cells were lysed in RIPA buffer supplemented with protease and phosphatase inhibitors. Western blotting of 30-μg protein lysate occurred using the following antibodies: p-PERK (T982, ref. 25) and ATF4 (Cell Signaling Technology, 1:1,000, catalog No. 11815, RRID:AB_2616025). Blots were imaged on a LiCor imager and normalized to total protein (Revert 700, Licor, 926–110210). Normalized band intensities were plotted as percent inhibition against a 10-point; threefold dilution series of HC-5404. IC_{50} values were calculated using 4-parameter logistic fitting in XLFit (IDBS, v5.5.0).

Protein analysis

Frozen pancreata from treated mice were homogenized and Western blotting was carried out with the following antibodies: phospho-PERK-T980 (1:1,000; ref. 25); total PERK (1:1,000, Cell Signaling Technology, catalog No. 3192, RRID:AB_2095847). Individual protein bands were quantitated using Image Lab Software (Bio-Rad Laboratories, v6.0; RRID:SCR_008426). Western blot data were compared by one-way ANOVA. Protein isolation and detection of pPERK and PERK using SimpleWestern was described elsewhere (23). In brief, protein detection was performed on the Jess SimpleWestern high-throughput protein analysis platform (ProteinSimple) according to the manufacturer's protocol using a 12- to 230-kDa Separation Module (ProteinSimple, SM-W004) and Total Protein Detection Module (ProteinSimple, DM-TP01). The following antibodies were used: p-PERK (Eli Lilly; 1:50), PERK (Cell Signaling Technology, 1:200, catalog No. 3192, RRID:AB_2095847), ASNS (ProteinTech, 1:200, catalog No. 14681–1-88; RRID:AB_2060119), CBS (ProteinTech, 1:100, catalog No. 14787–1-AP, RRID:AB_2070970), and CTH (ProteinTech, 1:100, catalog No. 60234–1-Ig, RRID:AB_2881358).

IHC and image analysis

Formalin-fixed paraffin-embedded samples were sectioned at 5-μm thickness and mounted on Superfrost Plus microscope slides (Thermo Fisher Scientific). IHC staining was performed on Bond Rx autostainer (Leica Biosystems) using the conventional TSA-amplified detection system. Primary antibodies used were as follows: α-CD31 (Abcam, catalog No. ab182981, RRID:AB_2920881), α-smooth muscle actin (SMA; Abcam, catalog No. ab124964, RRID:AB_11129103), and α-Meca32 (Novus Biologicals, catalog No. NB100–77668, RRID:AB_2276108). TSA-conjugated Alexa Fluor 488 and Alexa Fluor 647 fluorophores from Invitrogen (#B40953 and #B40958) were used at 1:500 dilution. Slides were counterstained with DAPI and coverslipped using Mowiol antifade mounting media (Sigma, #D2522). Slides were imaged with Aperio Versa 200 (Leica Biosystems) whole-slide scanner using 10x/0.32NA objective, and the data were analyzed using custom-written macros in ImageJ/FIJI (NIH; RRID:SCR_003070). Briefly, 150 μmol/L of the outer edges of the tumor sections were eliminated from the analysis. Gaussian-blurred DAPI channel was used to measure the area of the tissue. Scans of immunostaining were processed with median filter to remove noise, then positive areas were measured with appropriate threshold levels. The percentage of positive area for each marker was calculated. CD31-SMA double-positive areas were measured via image calculation of the binary images. One-way ANOVA and pairwise comparisons were performed on the data using Prism GraphPad.

Plasma protein binding

Equilibrium dialysis methods were used to determine the unbound fraction in female nu/nu mouse plasma obtained from Pharmaron Beijing Co. Ltd. Plasma samples spiked with 1 μmol/L HC-5404 or PBS, pH7.4 were placed in separate wells of a 96-well equilibrium dialysis plate (HTDialysis). The dialysis plate was placed in an incubator at 37°C with 5% CO_2 at approximately 100 rpm for 6 hours. After incubation, samples of plasma and buffer were matrix matched, quenched with acetonitrile (containing analytical internal standards), and centrifuged. Samples of the supernatant were analyzed for peak

area ratio by ultraperformance liquid chromatography-mass spectrometry (UPLC/MS-MS). The unbound fraction was determined using standard equations.

Pharmacokinetic bioanalysis in plasma and pancreas

PK/PD *in vivo* study was completed at MI Bioresearch (now part of Covance). Six- to 8-week-old female nude mice (athymic nude-Foxn1$_{nu}$; Envigo) were subcutaneously injected with 1×10^6 T-HEP3-PERK cells [PERK-overexpressing HEP3 human squamous cell carcinoma cell line provided by Julio Aguirre-Ghiso, Ph.D., professor (Albert Einstein College of Medicine)]. Tumors were allowed to grow to ∼200 mm^3 before receiving a single oral gavage dose of HC-5404 at 3 to 100 mg/kg, along with a vehicle of 20% (w/v) Captisol in 25 mmol/L NaH_2PO_4 buffer, pH 2. Blood, pancreas, and tumor tissues were collected at 1 to 24 hours postadministration ($n = 6$ per timepoint). PK/PD was evaluated in pancreas for 3 to 100 mg/kg groups at 1 to 12 hours postdose and in tumors after 1 hour. PK analysis of serum and pancreas was completed by Curia (formerly AMRI) and analyzed using LC/MS. For preparation and extraction of pancreas tissue homogenates, pancreas tissue samples were homogenized in Dulbecco's PBS (1:4 w/v) and Lysing Matrix D (MPBio, 116913050-CF) prior to LC/MS analysis. PK analysis was completed using Phoenix WinNonlin version 8.

Formulations and doses of compounds used in mouse studies

PERK inhibitor HC-5404 (lot No. 10000042C6) was manufactured at Albany Research Center (now known as Curia). HC-5404 was prepared in 20% (w/v) Captisol in 25 mmol/L $NaPO_4$ buffer, pH 2.0 as a solution or 0.5% methylcellulose (400 cp) in reverse osmosis in water as a suspension, depending on the study. Doses of HC-5404 used throughout the study are 3 to 100 mg/kg, given orally twice-a-day (every 12 hours). Sunitinib (Selleck, lot No. S778105) was solubilized in 5% DMSO in corn oil and used at a dose of 20 to 40 mg/kg, given orally once a day. Axitinib (Selleck, lot No. S100517) was solubilized in 0.5% carboxymethylcellulose (pH 2–3) and given twice-a-day (time interval of 8 hours) at 30 mg/kg by oral gavage. Lenvatinib (Selleck, lot No. S116402) was solubilized in 0.5% methylcellulose and used at a dose of 10 mg/kg, given orally once daily. Cabozantinib (Selleck, lot No. S111909) was dissolved in 30% propylene glycol: 5% Tween 80: 65% ddH_2O. and used at a dose of 30 mg/kg daily by oral gavage. DC-101 (BioXcell, lot No. 778620A2) was diluted to 1.5 mg/mL in PBS and administered at a dose of 15 mg/kg given twice a week by intraperitoneal injection. Fresh treatment formulations were prepared weekly throughout the duration of the study.

In vivo mouse tumor studies

Animal studies were conducted at Crown Bioscience, Charles River Discovery Research Services, and Covance. All procedures were conducted in compliance with the applicable laws, regulations, and guidelines of the NIH and with the approval of each of the institute's Animal Care and Use Committee. Female 6- to 8-week-old BALB/c nude mice (GemPharmatech Co. Ltd.), NOD.SCID (Beijing Anikeeper Biotech Co., Ltd.), and NMRI nude mice (Crl:NMRI-Foxn1nu) were used for *in vivo* studies. Animals were allowed to acclimate for 7 days upon arrival in an animal facility. Mice were housed in a 12-hour light/dark cycle facility under pathogen-free conditions with standard laboratory chow and water *ad libitum*.

Cell lines and culture

Cell lines 786-O (RRID:CVCL_1051), Caki-1 (RRID:CVCL_0234), A-498 (RRID: CVCL_1056), and Capan-2 (RRID:CVCL_0026) were obtained from ATCC. 786-O cells were cultured in RPMI (Gibco) + 10% FBS (Gibco) + 1% penicillin/streptomycin (Gibco), A-498 was cultured in MEM (Gibco) + 0.01 mmol/L NEAA (Gibco) + 10% FBS + 1% penicillin/streptomycin. Caki-1 and Capan-2 cells were cultured in McCoy's 5A media (Gibco) + 10% FBS + 1% penicillin/streptomycin. All cell lines were sent to a third party for STR authentication and PCR-based mycoplasma testing (IDEXX BioAnalytics). All cell lines are authenticated and confirmed negative for mycoplasma prior to any experimentation or *in vivo* transplantation.

Xenograft models

786-O cells (5×10^6 cells/mouse in 0.1 mL of PBS), A-498 (5×10^6 cells/mouse in 0.1 mL 1:1 PBS:Matrigel), Caki-1 (6×10^6 cells/mouse in 0.1 mL of PBS), and Capan-2 (1×10^7 cells/mouse in 0.1 mL 1:1 PBS: Matrigel) were implanted subcutaneously into the flank of animals for xenograft generation. Once average tumor volume reached 150 to 250 mm^3, animals were randomized by tumor size into groups of (8–10 animals) for treatment. After randomization, animals were typically dosed with the vehicle, HC-5404-FU in 0.5% methylcellulose (3, 10, or 30 mg/kg, orally, twice-a-day), Axitinib (15 or 30 mg/kg in 0.5% carboxymethylcellulose (pH 2–3, orally, twice-a-day), Lenvatinib (5 or 10 mg/kg in 0.5% methylcellulose, orally, twice-a-day), Cabozantinib (15, 30, or 60 mg/kg in 30% propylene glycol: 5% Tween 80: 65% ddH_2O, orally once-a-day), sunitinib (20 or 40 mg/kg in 5% DMSO in corn oil, orally once-a-day), or DC101 (15 mg/kg in PBS, i.p., twice a week).

Axitinib progression study

At the start of the study, 116 mice harboring 786-O xenografts (∼200 mm^3) began treatment with axitinib as a single agent (30 mg/kg, orally, twice-a-day). After 14 days of treatment, 77 mice bearing the largest tumors were rerandomized into four PD arms ($n = 8$), four efficacy arms ($n = 10$), and five tumors sampled on the day of rerandomization as a baseline. The remaining animals were removed from study. The four treatment groups were vehicle (0.5% methylcellulose), HC-5404 (30 mg/kg, orally, twice-a-day), axitinib (30 mg/kg, orally, twice-a-day), or the combination thereof, which continued for 28 days.

RCC PDX models

PDX studies were completed by Charles River Discovery Research Service. Fragments from 18 RCC PDX tumors were implanted subcutaneously into the flank of 4- to 6-week-old female NMRI nu/nu mice in the single mouse trial format ($n = 1$/group). Mice were randomized when tumors reached a range of 80 to 200 mm^3. Mice were treated with vehicle (0.5% methylcellulose), HC-5404 (30 mg/kg, orally, twice-a-day), axitinib (30 mg/kg, orally, twice-a-day), or a combination thereof for 28 days. Body weight and tumor volume were measured twice weekly. Tumor volume was calculated using the formula [tumor volume (mm^3) $= \pi/6 \times$ (length $\times$ width^2)] and plotted as means + SEM. Additional information on all PDX models used in this study are publicly available on the Charles River Tumor Model Compendium (http://compendium.criver.com).

The percentage of tumor growth inhibition was calculated at the end of the study using the formula: $100 \times [1 - (\Delta T/\Delta C)]$, if $\Delta T > 0$, ΔT, mean tumor volume of the drug-treated group on the observation day of the study – mean tumor volume of the drug-treated group on initial day of dosing; ΔC, mean tumor volume of the control group on the observation day of the study – mean tumor volume of the control group on initial day of dosing. Regression was calculated using the formula $= 100 \times \Delta T/T_{initial}$, if $\Delta T < 0$. Animals with ≥50% regressions were partial responders (PR). Animals with tumor volume of 0 (no measurable tumor) were considered as complete responders (CR),

and animals with less than 50% tumor regression and 30% growth over the baseline were considered to have stable disease (SD). Animals with tumors that increase by more than 30% over the baseline were considered to have progressive disease (PD). The percent change in body weight was calculated by the formula (body weight on observation day – body weight on initial day)/body weight on initial day × 100%.

Statistical analyses

To determine the significance of the *in vivo* data using statistical methods, we compared the final tumor volumes of different groups. Bartlett test was used to check the assumption of homogeneity of variance across all groups. When the *P* value of Bartlett test is ≥0.05, we ran one-way ANOVA to test overall equality of means across all groups followed by Tukey and Dunnett. When the *P* value of Bartlett test was <0.05, we ran Kruskal–Wallis test to test the overall equality of medians among all groups. If the *P* value the Kruskal–Wallis test was <0.05, we further perform post hoc testing by running Conover's nonparametric test for all pairwise comparisons or for comparing each treatment group with the vehicle group, both with single-step *P* value adjustment. All statistical analyses were performed using Prism software (Graphpad Prism, Version 9.5.1, RRID:SCR_002798). All tests were two-sided unless otherwise specified, and *P* values of <0.05 were regarded as statistically significant.

Data availability statement

Data generated in this study are available within the article and its supplementary data files. All other data are available from the corresponding author upon reasonable request.

Results

HC-5404 is a potent and selective PERK inhibitor

PERK is one of four closely related ISR kinases that phosphorylate eIF2α in response to cellular stress (26). Both tumorigenesis and treatment with many anticancer agents have been shown to activate ISR (27, 28), and hypoxic stress is associated with activation of PERK signaling as an adaptive response (16, 19, 20). To understand the specific role of PERK in RCC, we have employed the aminopyridine PERK inhibitor HC-5404 (formerly LY-4; **Fig. 1A**; refs. 22, 29, 30).

Cell-free biochemical assays were used to evaluate the selectivity of HC-5404 for PERK, relative to the other ISR kinases GCN2 (EIF2AK4), HRI (EIF2AK1), and PKR (EIF2AK2; ref. 26). In these assays, recombinant target kinases were incubated with ATP and an eIF2α-based fluorogenic substrate; kinase activity was evaluated in the presence of HC-5404 across a concentration series (22, 23). These experiments revealed an IC_{50} for PERK of 1 nmol/L, representing a >2,000-fold biochemical selectivity over GCN2 (IC_{50} = 2.17 μmol/L), HRI (IC_{50} = 2.96 μmol/L), and PKR (IC_{50} > 10 μmol/L; **Fig. 1B**; Supplementary Fig. S1A). The selectivity of HC-5404 against the broader kinome was then evaluated using a KINOMEScan binding panel assay that measured the interaction with 468 unique kinases, including 403 wild-type (WT) human kinases and 59 mutant isoforms (24). Notably, the kinome panel does not include PERK. HC-5404 was evaluated at 100, 1,000, and 10,000 nmol/L, which revealed a high level of selectivity across the kinome (**Fig. 1C**; Supplementary Fig. S1B). There were no interactions with human kinases observed when HC-5404 was assayed at 100 nmol/L, whereas only five kinases were inhibited >50% when HC-5404 was tested at 1,000 nmol/L, including BLK, MER, mutant RET(M918T), and the atypical kinases RIOK1 and RIOK2. Although 27 interactions were reported when assayed at 10,000 nmol/L, only nine kinases were inhibited greater than 65% (see Supplementary Table ST1 for Complete KINOMEScan Results).

The cell-based activity of HC-5404 was evaluated using HEK-293 treated with 1 μmol/L tunicamycin (Tm) to induce ER stress. Tm treatment resulted in PERK autophosphorylation at Thr982 (pPERK) and increased ATF4 levels, both of which were inhibited by HC-5404 in a concentration-dependent manner *in vitro* (IC_{50} = 23 and 88 nmol/L, respectively; **Fig. 1D**). Taken together, these results validate HC-5404 as a potent and selective inhibitor, with good cell-based activity, consistent with previously published results (22, 30).

In vivo characterization of HC-5404 as orally bioavailable and active in xenograft models

Initial *in vivo* studies were aimed at understanding the pharmacokinetic and pharmacodynamic (PK/PD) relationship and optimizing the dosing regimen. HC-5404 was quantified from mouse plasma following a single oral administration (PO) at doses ranging from 3 to 100 mg/kg. Dose-proportional increases in exposure were observed up to 100 mg/kg, reaching a maximum concentration (C_{max}) before 1 hour and an average half-life of 2.22 hours (Supplementary Table ST2). Unbound fraction in mouse plasma was determined *in vitro* to be 2.3%, which enabled us to calculate the free or unbound drug plasma exposure across time *in vivo* (**Fig. 2A**; Supplementary Fig. S2A). Oral dosing at 30 and 100 mg/kg resulted in C_{max} free drug concentrations of 186 and 839 nmol/L, respectively. Even at the highest dose tested (100 mg/kg), the free drug concentration was below the 1,000 nmol/L concentration assayed in the kinome scan that revealed minimal binding to secondary targets.

The PK/PD relationship was evaluated in mouse pancreas, as the pancreas has high levels of basal pPERK activity that makes it suitable for PD analysis (31). Treatment with HC-5404 resulted in a time- and dose-dependent inhibition of pPERK in pancreas tissue. Following a single oral administration of HC-5404 at 30 mg/kg, pPERK inhibition in the mouse pancreas was approximately 90% at the early timepoints after dosing (**Fig. 2B**). As HC-5404 is cleared from plasma, pPERK gradually increased until basal levels were restored by 12 hours after dosing. Single oral administration at 100 mg/kg achieved a proportional increase in exposure from the 30-mg/kg dose, maintaining exposure above 3,220 ng/mL (163 nmol/L, unbound) in plasma up to 12 hours after dosing and resulting in near-complete pPERK inhibition (>80% inhibition) for the first 12 hours following treatment (**Fig. 2B**).

The ability of HC-5404 to suppress tumor growth was evaluated in the 786-O xenograft model of RCC, which is a highly vascularized tumor model sensitive to PERK inhibition (22, 23). The 786-O tumor model is homozygous for a frameshift mutation following Gly104 in von Hippel-Lindau protein (*VHL*), resulting in HIF stabilization and activation of unfolded protein response (UPR), including elevated pPERK (32, 33). Similar to the pancreas, administration of 30 mg/kg HC-5404 induced ∼90% pPERK inhibition in 786-O tumors at 1 hour, which returned to baseline by 8 hours (Supplementary Fig. S2B).

To evaluate the single-agent activity of HC-5404 and explore the effect of fractioning the dose between once-a-day and twice-a-day dosing, mice harboring 786-O xenografts were treated with 3, 10, or 30 mg/kg orally twice-a-day dosing alongside 6, 20, or 60 mg/kg orally twice-a-day dosing to evaluate the effect of the dose regimen on tumor growth. The differences between twice-a-day and once-a-day dosing were not statistically significant, but the general trend indicated better antitumor activity with twice-a-day dosing. Of the doses tested, 30 mg/kg twice-a-day induced the greatest effect resulting in 48% tumor growth inhibition (TGI; **Fig. 2C**; Supplementary Fig. S2C).

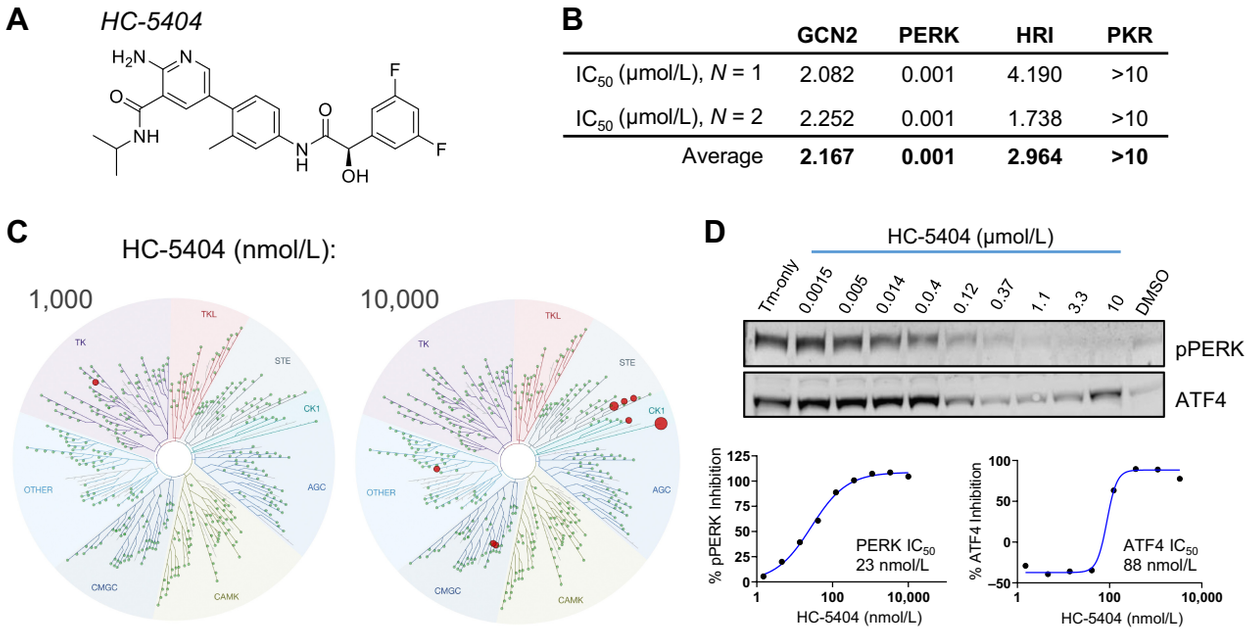

	GCN2	PERK	HRI	PKR
IC_{50} (μmol/L), $N = 1$	2.082	0.001	4.190	>10
IC_{50} (μmol/L), $N = 2$	2.252	0.001	1.738	>10
Average	**2.167**	**0.001**	**2.964**	**>10**

Figure 1.

Biochemical and cell-based characterization of HC-5404 as a potent and selective PERK inhibitor. **A,** HC-5404 molecular structure. **B,** IC_{50} values for four closely related ISR kinases determined by FRET-based biochemical assays. **C,** Biochemical TreeSpot kinome panel assays demonstrate selectivity of HC-5404 against >400 kinases. NB: PERK is not included in the panel, and no interactions were observed when HC-5404 assayed at 100 nmol/L. Image generated using TREEspot Software Tool. Reprinted with permission from KINOMEscan, a division of DiscoveRx Corporation, © DISCOVERX CORPORATION 2010. **D,** Western blot analysis of pPERK and ATF4 in HEK-293 cells treated with HC-5404 in the presence of 1 μmol/L tunicamycin. HEK-293 cells treated with HC-5404 across a threefold dilution series ranging from 1.5 nmol/L to 10 μmol/L. Quantification of Western blot used to generate IC_{50} values: pPERK IC_{50} = 23 nmol/L; inhibition of ATF4 IC_{50} = 88 nmol/L.

CAPAN-S2 pancreatic tumor xenografts, another model previously reported to be sensitive to PERK inhibition (31), were treated with 30 and 100 mg/kg HC-5404 twice-a-day, resulting in TGI of 50% and 43%, respectively (**Fig. 2D**). No difference between the dose levels was observed, suggesting that increasing doses above 30 mg/kg, when administered twice per day, was not likely to improve the single-agent activity of HC-5404. As PERK inhibition has been associated with pancreatic toxicity (31), pancreas sections were evaluated from mice treated with 30 or 100 mg/kg HC-5404. Histologic evaluation of collected pancreas revealed changes only in the 100 mg/kg dose, which were reversible with a 2-week washout period (Supplementary Fig. S2D). Taken together, these findings further supported the decision to dose HC-5404 at 30 mg/kg, orally twice-a-day in all subsequent *in vivo* studies.

HC-5404 sensitizes RCC tumor models to VEGFR-TKI

As hypoxia and glucose deprivation are known drivers of ER stress and PERK-mediated adaptive responses (18, 20), we hypothesized that HC-5404 would sensitize RCC tumor models to antiangiogenic VEGFR-TKI. Initial studies with sunitinib revealed that VEGFR-TKI induced pPERK in 786-O xenografts and that this effect increased over time (Supplementary Fig. S2E). Next, we evaluated the impact of three second-generation VEGFR-TKI on tumor growth and PERK activation. Cabozantinib, lenvatinib, or axitinib were orally administered at multiple doses to mice harboring 786-O xenografts for 21 days, after which the tumors were resected and analyzed for pPERK levels (Supplementary Figs. S3A–S3C). All three VEGFR-TKI induced dose-dependent increases in pPERK levels that corresponded to the level of tumor growth inhibition (Supplementary Figs. S3D–S3F), and none of the VEGFR-TKI induced body weight loss at the doses tested (Supplementary Figs. S3G–S3I). On the basis of these experiments, dose regimens for each VEGFR-TKI were selected for follow-up combination studies.

Having demonstrated that VEGFR-TKI induce pPERK, we next tested whether the addition of HC-5404 enhanced the antitumor effect of these agents. Axitinib, cabozantinib, lenvatinib, and sunitinib were each tested in combination with HC-5404 in 786-O RCC xenografts. All studies included a PD arm that was sampled after 7 days of dosing to analyze the effect of treatments on angiogenesis and pPERK levels. Consistent with our initial dose-determining studies, the PD arms of the experiments revealed that all VEGFR-TKI induced pPERK accumulation, which were inhibited by the addition of HC-5404 (**Fig. 3A**; Supplementary Fig. S2F). In the efficacy arms of each tumor growth study, HC-5404 and the second-generation VEGFR-TKI (axitinib and cabozantinib) resulted in modest effects on tumor volume as monotherapies. In contrast, when the VEGFR-TKI were combined with HC-5404, tumors regressed relative to baseline (**Fig. 3B**). Lenvatinib and sunitinib as single agents were effective inhibitors of 786-O growth, yet the combination with HC-5404 still enhanced the level of TGI. No significant mouse body weight loss was observed across any of the combination studies (Supplementary Figs. S4A–S4D). PK analysis of HC-5404 and sunitinib revealed that neither of these two agents affects the exposure of the other, confirming that the increased activity of the combination is a mechanistic interaction rather than a PK-driven effect (Supplementary Fig. S4E and S4F).

The effect of HC-5404 was further validated in tumors by assessing the response of markers of *in vivo* PERK inhibition. Previous studies have highlighted a surprising induction of downstream targets of ATF4, including asparagine synthetase (ASNS) and phosphoserine aminotransferase (PSAT1; ref. 31). We evaluated whether these

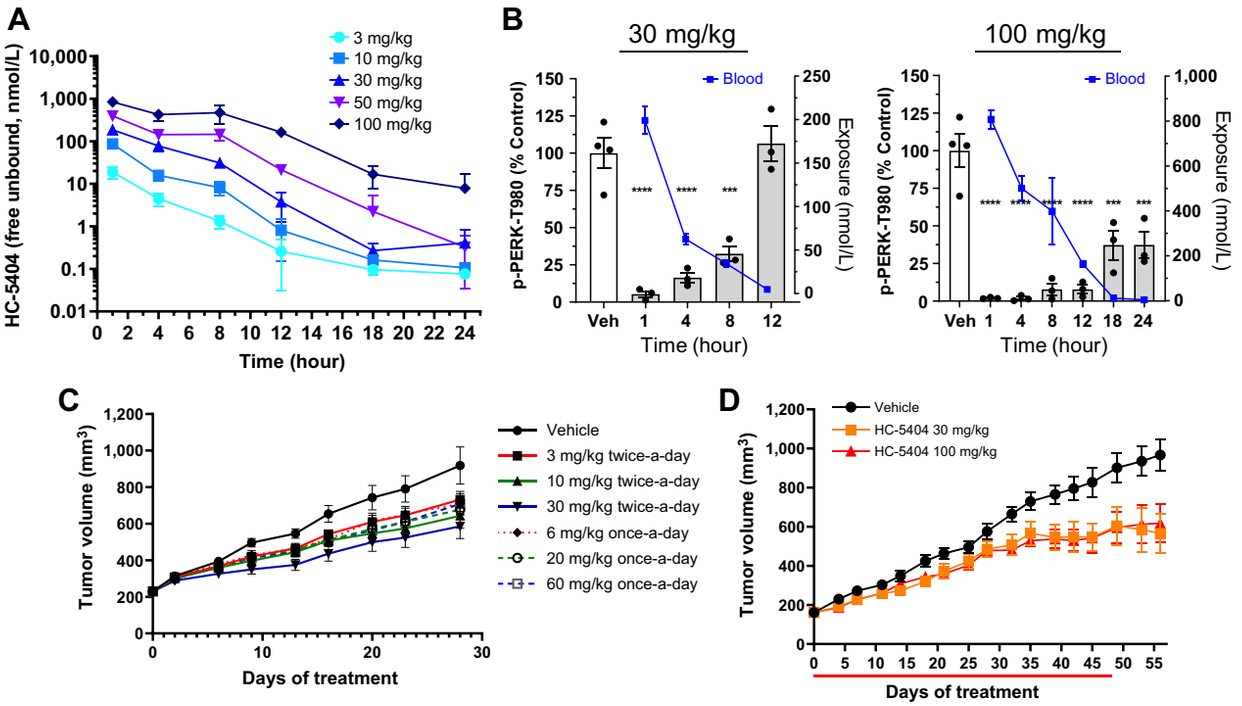

Figure 2.

In vivo characterization of HC-5404. **A,** Free drug levels of HC-5404 in mouse plasma following single oral administration (PO). Plasma sampled across a 24-hour period and quantified by LC/MS-MS. Data represent mean ± SEM, $n = 3$ mice per group. **B,** Mouse pancreas pPERK levels and plasma exposure following oral administration of HC-5404 at 30 and 100 mg/kg. Data represent mean ± SEM, $n = 3$ mice per group. **C,** 786-O xenografts treated with HC-5404 at multiple dose levels and treatment regimens for 28 days. Values represent mean tumor volume ± SEM, $n = 10$ mice per group. Statistical analysis of final tumor volume found in Supplementary Fig. S2C. **D,** Mice harboring subcutaneous CAPAN-2 pancreatic tumor xenografts treated with HC-5404 at 30 and 100 mg/kg orally twice-a-day for 48 days ($n = 10$ mice per group).

changes were consistent with our studies by testing these alongside other canonical targets of ATF4, including cystathionine beta synthase (CBS) and cystathionine gamma lyase (CTH; ref. 34). Treatment with HC-5404 induced a dose-dependent accumulation of ASNS, CBS, and CTH in 786-O tumors (**Fig. 3C**), likely reflecting enhanced tumor stress caused by blocking PERK in tumors. Although consistent with previous investigations into small molecule PERK inhibitors, the specific mechanism behind the *in vivo* activation of ATF4 remains unclear.

Combining HC-5404 with VEGFR-TKI improves response across diverse RCC tumor models

RCC is frequently characterized by mutations in and epigenetic silencing of *VHL*, which results in dysregulated HIF expression that drives a proangiogenic tumor environment associated with activated UPR (32, 33). It is possible that *VHL* mutation status, pPERK expression, and sensitivity to VEGFR-TKI may be linked, so we made use of three well-characterized RCC tumor models to explore the effect of VHL status on HC-5404 sensitivity. To this end, 786-O and A-498 (Gly144 frameshift) were selected as representative of *VHL*-mutant models, and Caki-1 was chosen as a *VHL* WT model (35).

To evaluate differences in sensitivity to PERK inhibition and VEGFR-TKI treatments, A-498 and Caki-1 models were treated with HC-5404, sunitinib, or a combination thereof for 28 days. In the three models tested, tumor response reflected the genetic background: the *VHL*-mutant A-498 was sensitive to HC-5404 as a single agent, although the TGI only reached ∼40% (**Fig. 4A**). Similarly, the A-498 model was sensitive to sunitinib with robust single-agent activity that resulted in 80% TGI. When sunitinib and HC-5404 were combined in A-498, tumor regression of 22% was observed (**Fig. 4A**). In contrast, Caki-1 was far less sensitive to either HC-5404 or sunitinib as a monotherapy. Although an effect of the combination treatments was observed, the TGI only reached 47% in the combination group (**Fig. 4B**). On the basis of this finding, we decided to assess the level of response in VHL WT models more generally and determine whether VHL mutation status was a reliable marker of tumor sensitivity to the combination treatment. Consistent with the HIF pathway activation resulting from *VHL* mutation driving ER stress, 786-O and A-498 tumors had elevated levels of pPERK in the vehicle group (**Fig. 4C**), whereas pPERK was barely detectible in Caki-1. As expected, HC-5404 inhibited pPERK expression across the three models.

One limitation of cell-line–derived xenograft (CDX) studies is homogeneity across the tumor tissue, which is not reflective of the cellular diversity expected in patient tumors. To overcome this limitation, we made use of 18 RCC patient-derived xenograft (PDX) models to evaluate the activity of HC-5404 and VEGFR-TKI across a diverse panel of clinically relevant tumor models in a single animal study ($n = 1$). In contrast with CDX models, low-passage PDX maintain tissue architecture that reflects the primary tumor from which they were derived (36). Importantly, the sensitivity of subcutaneous PDX models to systemic treatments correlates closely with matched patient responses (36, 37). This study included six models that were VHL WT to test whether VHL mutation status could be used as a marker of HC-5404 and VEGFR-TKI sensitivity. Animals were

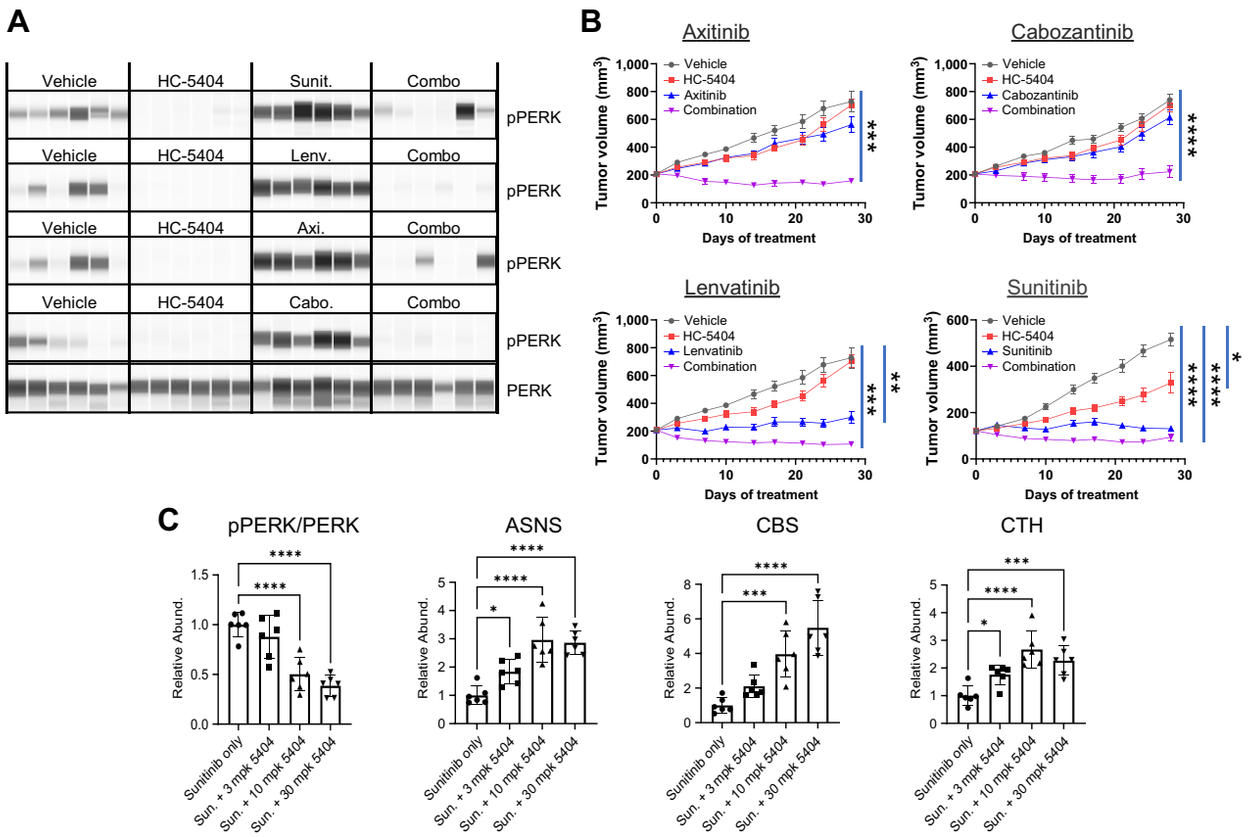

Figure 3.

HC-5404 combines with VEGFR-TKI to inhibit tumor growth in 786-O xenograft models of RCC. **A,** Protein analysis of pPERK and PERK in 786-O xenografts treated with VEGFR-TKI. Samples taken from studies in **B** after 7 days of treatment. **B,** 786-O tumor xenografts treated with HC-5404 (30 mg/kg; orally, twice-a-day), sunitinib (40 mg/kg; orally, once-a-day), lenvatinib (10 mg/kg; orally, once-a-day), axitinib (30 mg/kg; orally, twice-a-day), or cabozantinib (30 mg/kg; orally, once-a-day) and combinations as indicated for 28 days. Data presented in the axitinib, cabozantinib, and lenvatinib panels were generated together in a large, multiarmed *in vivo* study. As such, data from vehicle groups and HC-5404 arms are replicated in both the axitinib and lenvatinib panels, as these VEGFR-TKI used the same vehicle control. Sunitinib was run in a separate study. Note that variability from study-to-study is reflected in tumor growth curves without affecting the conclusions. Final tumor volume analyzed by Welch ANOVA or one-way ANOVA following homogeneity of variance tests. Data represent mean ± S.E.M., $n = 10$ mice per group (*, $P < 0.05$; **, $P < 0.01$; ***, $P < 0.005$; ****, $P < 0.001$). **C,** Protein analysis of pPERK, PERK, ASNS, CBS, and CTH in xenograft samples treated with sunitinib and HC-5404 at indicated doses. Statistical analysis by ANOVA one-way following homogeneity of variance tests (*, $P < 0.05$; **, $P < 0.01$; ***, $P < 0.005$; ****, $P < 0.001$).

treated with axitinib, HC-5404, or the combination thereof for 28 days, and scored for the magnitude of response to the combination group. The models were ranked based on change in tumor volume relative to starting baseline and scored for the number of partial responses (PR). In this case, PR was considered as a regression in volume equal or greater than 50% compared with baseline. Although axitinib as a monotherapy resulted in two of 18 PR, the combination of HC-5404 with axitinib resulted in nine of 18 PR (**Fig. 4D**; Supplementary Table ST3).

Three of the six *VHL* WT models responded to the combination treatment with notable improvement over axitinib monotherapy (**Fig. 4D**; Supplementary Table ST3). Of the six *VHL* WT models tested, two of six resulted in PR, two of six models had stable disease (SD), and two of six models resulted in PD in response to the combination treatment. Importantly, the two models that had PD exhibited greater response to the combination treatment relative to the monotherapies. In these two models (RXF-393 and RXF-2540), a combination benefit was conferred by the two treatments despite lower overall sensitivity of the two models. Two *VHL* WT models did not respond to the combination benefit at all but were sensitive to axitinib as a single agent, resulting in tumor stasis in response to axitinib monotherapy (RXF-1220 and MRI-H-166). In contrast, SMTCA75 was a VHL WT PDX model that responded to combination treatment with 53% regression, yet tumor stasis in response to axitinib monotherapy.

Consistent with observations in the three CDX models, the VHL-mutant PDX models had a modest but significantly higher basal level of pPERK activation in pretreated baseline samples (**Fig. 4E**), further highlighting the link between VHL status and pPERK activation in RCC. As the VHL WT models appeared less sensitive to combination treatments overall (left side of waterfall plot, **Fig. 4D**), we wanted to assess whether VHL mutation status could be developed into a predictive biomarker of tumor sensitivity. In terms of percent change in final tumor volume, the VHL WT models were less sensitive to the combination treatment following 28 days of treatment (**Fig. 4F**). However, some models were notably less sensitive to axitinib monotherapy, while still exhibiting substantial improvement to the

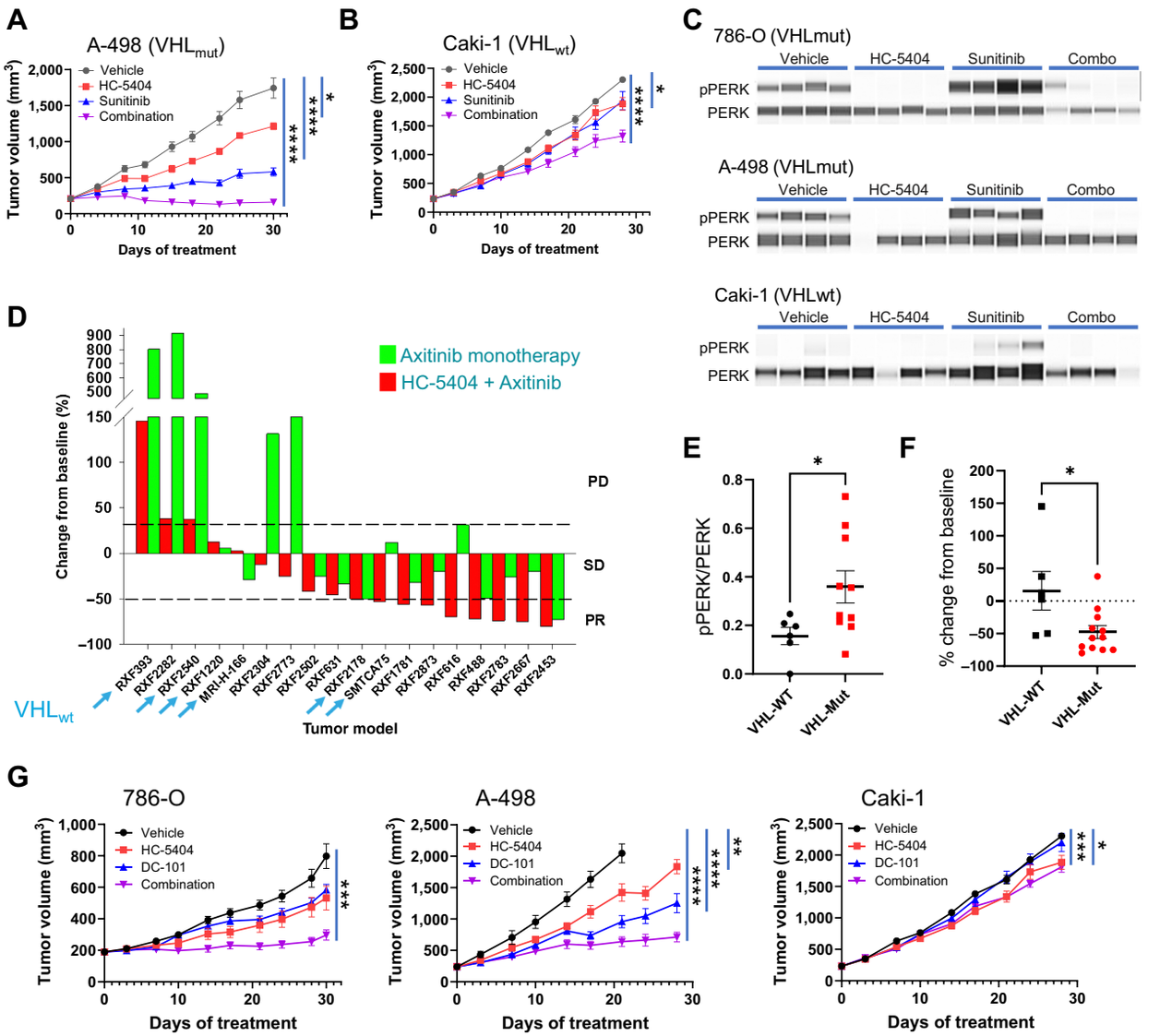

Figure 4.

Sensitivity to VEGFR-TKI and HC-5404 combination is independent of *VHL* mutation status. **A** and **B,** A-498 and Caki-1 RCC tumor xenografts treated with HC-5404 (30 mg/kg; orally, twice-a-day) and sunitinib (20 mg/kg; orally, once-a-day) for 30 days. Final tumor volume analyzed by Welch ANOVA or one-way ANOVA following homogeneity of variance tests. Data represent mean ± S.E.M., $n = 10$ mice per group (*, $P < 0.05$; ****, $P < 0.001$). **C,** pPERK and PERK abundance evaluated by SimpleWestern in RCC tumor xenografts treated for 7 days with HC-5404 (30 mg/kg; orally, twice-a-day), sunitinib (20 mg/kg in Caki-1 and A-498; 40 mg/kg in 786-O; orally, twice-a-day), or a combination thereof. **D,** Waterfall plot illustrating relative change in tumor volume of 18 diverse RCC PDX models following 28 days of treatment in a single animal ($n = 1$/group/model) with either axitinib (30 mg/kg; orally, twice-a-day), HC-5404 (30 mg/kg; orally, twice-a-day), or a combination thereof. Models ranked on % change tumor volume in combination group. PD = >30% increase from baseline; stable disease (SD) = ≤30% increase from baseline and <50% regression; PR = ≥50% regression. Models that are *VHL* WT are indicated by an arrow. **E,** Quantification of pPERK and PERK protein levels by SimpleWestern from pretreatment baseline PDX tumor samples. Y-axis represents arbitrary fluorescence units. Differences in pPERK/PERK levels evaluated by Student *t* test, *, $P < 0.05$ (VHL-WT $n = 6$; VHL-MUT $n = 11$). **F,** Final tumor volume of 18 RCC PDX models following 28 days of treatment with HC-5404 (30 mg/kg, orally, twice-a-day) and axitinib (30 mg/kg, orally, twice-a-day). Differences in tumor volume evaluated by Student *t* test; *, $P < 0.05$ (VHL-WT: $n = 6$; VHL-MUT: $n = 12$). **G,** RCC CDX tumor models treated with HC-5404 (30 mg/kg orally, twice-a-day) and DC-101 (15 mg/kg; i.p., twice a week) for 28 days. Tumor volume on day 28 (786-O, Caki-1) or day 21 (A-498) was analyzed by Welch ANOVA or one-way ANOVA following homogeneity of variance tests. Data represent mean ± S.E.M., $n = 10$ mice per group (*, $P < 0.05$; **, $P < 0.01$; ***, $P < 0.005$; ****, $P < 0.001$).

combination treatments relative to monotherapy (RXF-393 and RXF-2540). It was concluded that VHL mutation may be associated with enhanced sensitivity to the combination treatments, but the VHL WT tumors still benefited from addition of HC-5404 to the axitinib regimen.

HC-5404 demonstrates combination benefit with other agents targeting angiogenesis

Although the common target associated with antiangiogenic activity is inhibition of the VEGF axis, the secondary targets of the VEGFR-TKI have been proposed to improve antitumor activity (7, 10). To test

whether inhibition of the VEGF/VEGFR axis is sufficient to drive the combination benefit with HC-5404, we made use of a mouse mAb, which selectively targets mouse VEGFR-2. DC-101 is a surrogate mAb to human anti-VEGFR2 mAb, ramucirumab, that is approved for use in multiple cancer types (38). We tested whether treatment with HC-5404 could enhance the activity of DC-101 across three models of RCC (786-O, A-498, and Caki-1). Similar to the observations of HC-5404 with VEGFR-TKI, the combination treatment improved the effects of each monotherapy in 786-O and A-498 xenografts with TGI values of 82% and 78%, respectively (**Fig. 4G**). In contrast, cotreatment of DC-101 and HC-5404 did not exhibit significant combination benefits resulting in a TGI value of only 24% in Caki-1 following 28 days of treatment (**Fig. 4G**). Unlike the VEGFR-TKI, the combination treatment with DC-101 did not result in tumor regression in any of the models tested.

PERK enhances the antiangiogenic effects of VEGFR-TKI

PERK is an adaptive stress response that links hypoxia and nutrient deprivation with proangiogenic signaling (16, 18, 20), so we evaluated the effect of HC-5404 on tumor vasculature when administered in combination with antiangiogenic VEGFR-TKI. IHC staining of tumor sections confirmed that axitinib decreased the proportion of Meca32 (also called PLVAP) expressing vascular endothelial cells and that this effect was enhanced by the addition of HC-5404 (**Fig. 5A** and **B**). Notably, HC-5404 alone did not affect this vascular endothelium

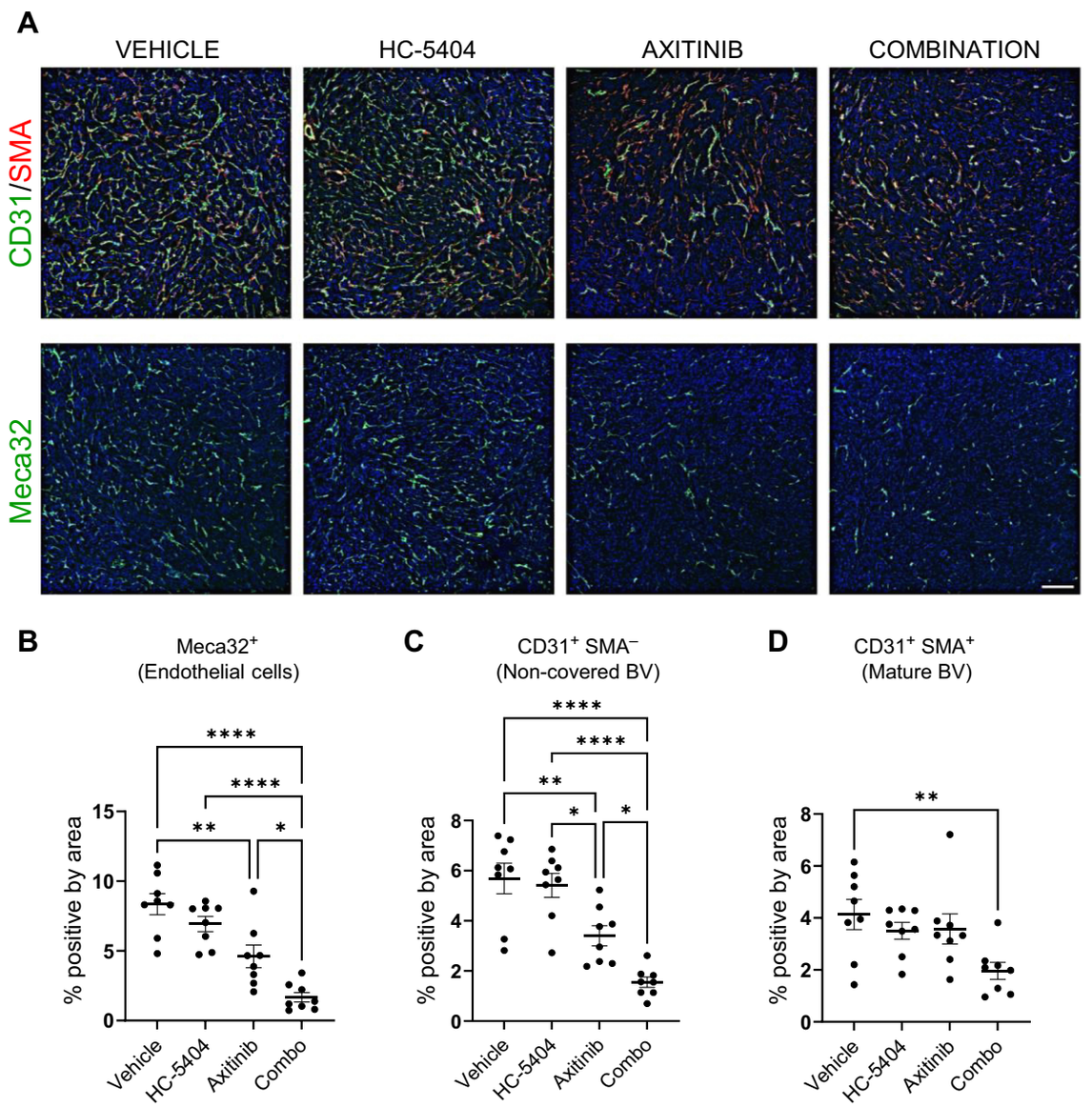

Figure 5.

HC-5404 sensitizes 786-O xenografts to the antiangiogenic effects of axitinib. **A,** IHC images of 786-O xenograft sections stained with antibodies specific to Meca32, CD31, and SMA. Scale bar = 150 μm. HC-5404 and axitinib administered at 30 mg/kg, twice-a-day for 7 days. **B–D,** Quantification of IHC staining of xenograft sections. Graphs indicate proportion of cells stained positive for Meca32, positive for CD31 in absence of SMA (%$CD31^+SMA^-$), or cells that stain positive for both CD31 and SMA (%$CD31^+SMA^+$). One-way ANOVA statistical analysis evaluated differences between treatment groups; asterisks indicate significant differences (*, $P < 0.05$; **, $P < 0.01$; ****, $P < 0.001$).

marker, highlighting a context-dependent effect of HC-5404 on tumor angiogenesis.

As immature blood vessels mature, they develop a mural layer of cells that express smooth muscle actin (SMA), which encircles and stabilizes the maturing vessel (39). By costaining for both CD31 and SMA, we assessed whether treatments were affecting mature or immature tumor blood vessels. Similar to effects observed with the endothelial marker Meca32, axitinib as a single agent decreased the proportion of immature $CD31^{+}SMA^{-}$ vessels, an effect that was enhanced by the addition of HC-5404 (**Fig. 5C**). In contrast, axitinib did not affect the number of mature $CD31^{+}SMA^{+}$ cells at the dose and time points analyzed, consistent with the predominant role that VEGF/VEGFR axis plays in the production of new vasculature (40). HC-5404 as a single agent did not affect the expression of any vascular markers tested, whereas the combination treatments resulted in a significant decrease in mature $CD31^{+}SMA^{+}$ blood vessel cells (**Fig. 5D**).

PERK is a vulnerability for RCC xenografts that have progressed on VEGFR-TKI

Despite initial responses to VEGFR-TKI therapy, tumor regrowth necessitates subsequent rounds of alternate therapies to improve patient outcomes (12). We modeled this effect by challenging 786-O xenografts to progress on axitinib treatment for 2 weeks, then transferred resistant (nonresponder) mice to one of four treatment groups. This enabled us to test whether adding HC-5404 to the treatment regimen could drive combination benefits despite having previously progressed on axitinib alone. Animals that were transferred to the vehicle group experienced an increase in growth rate, suggesting that although the tumors had advanced on axitinib, some sensitivity to treatment remained. Groups that were transferred to single-agent axitinib or HC-5404 groups progressed at approximately the same rate as prior to rerandomization. By the end of the study, single-agent activity of HC-5404 or axitinib inhibited tumor growth by 47% or 38%, relative to vehicle (**Fig. 6A**). When HC-5404 was added to the axitinib regimen in the combination group, xenografts regressed in volume following a brief period of continued growth, resulting in average tumor regression of 20% relative to baseline (**Fig. 6A**). Thus, tumors that have previously progressed on axitinib remain sensitive to HC-5404 when administered in combination with the VEGFR-TKI.

Consistent with the findings noted above, axitinib decreased the number of $Meca32^{+}$ and $CD31^{+}SMA^{+}$ cells in xenograft sections,

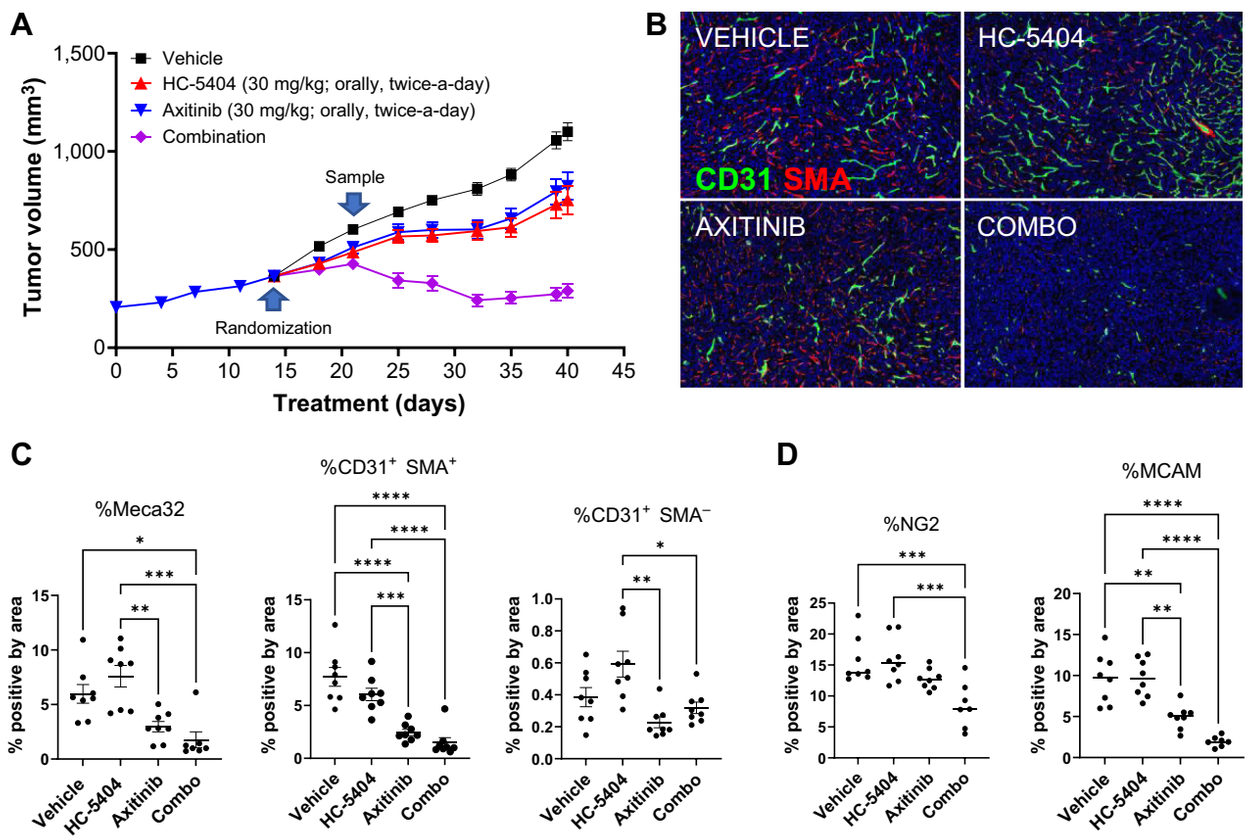

Figure 6.

Addition of HC-5404 to axitinib regimen induces tumor regression. **A,** 786-O tumor growth across the study period. Xenografts that progressed in presence of axitinib for 14 days were rerandomized and transferred to indicated treatment groups for an additional 28 days. Data represent mean ± S.E.M. Final tumor volume analyzed by Welch ANOVA. Data represent mean ± S.E.M., $n = 8$ mice per group (**, $P < 0.01$; ***, $P < 0.005$; ****, $P < 0.001$). **B,** IHC images of xenograft sections stained with antibodies specific for CD31 and SMA. **C,** Quantification of proportion of cells that stained positive for Meca32, CD31+SMA- (immature blood vessels), or $CD31^{+}SMA^{+}$ (mature blood vessels) in **B**. One-way ANOVA was used to evaluate the statistical significance between groups. Asterisks indicate statistical significance (*, $P < 0.05$; **, $P < 0.01$; ***, $P < 0.005$; ****, $P < 0.001$). **D,** Quantification of IHC staining of tumor sections using antibodies specific for the pericyte markers NG2 and MCAM. One-way ANOVA statistical analysis evaluated differences between treatment groups; asterisks indicate significant differences (**, $P < 0.01$; ***, $P < 0.005$; ****, $P < 0.001$).

which was enhanced by the addition of HC-5404 to the combination group (**Fig. 6B** and **C**). $CD31^{+}SMA^{-}$ (immature blood vessels) were nearly absent across the four groups, likely depleted during the initial 2-week axitinib treatment. Pericytes form a layer of mural cells that surround blood vessels, and are important for vascular morphogenesis and branching (41). Two pericyte markers (NG2 and MCAM; ref. 44) were used to evaluate the effect of axitinib and HC-5404 on the pericyte layer. The proportion of cells that stained positive for $NG2^{+}$ decreased only in the combination group relative to vehicle, highlighting the impact of the combination treatment on the pericyte layer. $MCAM^{+}$ cells were decreased by axitinib, and this effect was enhanced by the addition of HC-5404 (**Fig. 6D**; Supplementary Fig. S5). In both cases, the proportion of $NG2^{+}$ and $MCAM^{+}$ cells were decreased relative to the baseline samples, suggesting that following rerandomization the tumors in the combination group underwent a loss of mature vascular cells, rather than simply inhibition of neovascular growth.

Discussion

Antiangiogenic VEGFR-TKI inhibit tumor vascular formation, disrupting the flow of oxygen and nutrients to tissues, thereby driving PERK activation as part of a concerted adaptive stress response. Here we demonstrate that blocking PERK sensitizes xenografts to multiple VEGFR-TKI across diverse tumor models of RCC, resulting in enhanced vascular inhibition and tumor regression. VEGFR-TKI form the backbone of standard of care in RCC, either as monotherapies or in combination with immune checkpoint inhibitors (NCCN, 2023; ref. 13). Our findings support a clinical opportunity to enhance the standard of care in RCC and improve patient outcomes.

Patients often experience promising initial responses to VEGFR-TKI, but their tumors frequently progress, necessitating multiple rounds of VEGFR-targeting agents (12). This medical need has resulted in many publications attempting to improve VEGFR-targeting agents using subcutaneous xenograft models, but the clinical predictiveness of these studies has come into question, especially since these models are highly dependent on neovascularization (42). For example, Guerin and colleagues propose different approaches to improve the clinical predictive value, notably exploring models that capture better the impact of the novel agents on mature vasculature and leveraging PDX and GEMM studies to understand the effects of tumor microenvironment heterogeneity (42). To understand the impact of the HC-5404/VEGFR-TKI combination on mature vasculature, we allowed tumors to progress on axitinib to establish normalized mature vasculature under the influence of the VEGFR-TKI. Remarkably, addition of HC-5404 to axitinib resulted in regression of ~20% in the combination group. IHC demonstrated that these responses were associated with diminished mature blood vessels and pericyte cells. In addition, we have included an 18-model PDX study, where we have demonstrated broad-spectrum improvement of responses for the combination over axitinib single-agent activity. We believe that these additional studies address important limitations experienced in typical published xenograft studies.

One mechanism through which tumors can overcome inhibitory effect of antiangiogenic VEGFR-TKI is through vessel co-option (VCO) of the preexisting healthy vasculature to deliver oxygen and nutrients to the growing tumor (43, 44). RCC is a highly vascularized tumor that relies on angiogenesis to support tumor growth and while there are examples of VCO enabling RCC lung metastases, VCO occurs less frequently in RCC metastases relative to other cancers (45). As VCO often occurs at alveolar sites, future investigation into VCO as a potential resistance mechanism to HC-5404 and VEGFR-TKI is warranted to support a translational program beyond RCC, particularly in cancers that frequently metastasize to the lungs (43, 44).

Combination benefit was observed in response to either multi-targeted small molecule VEGFR-TKI or the VEGFR2-specific mAb DC-101, demonstrating that much of the effect is mediated through the VEGFR2 axis. Although the VEGF/VEGFR axis is a key driver to the combination benefit, secondary targets of VEGFR-TKI likely contribute to more robust combinatorial effects that result in tumor regression. Importantly, the ability of HC-5404 to enhance the activity of all VEGF/VEGFR inhibitors tested highlights of the interchangeability of the VEGFR-inhibiting agent and general applicability of PERK inhibitors across the entire therapeutic class. There are many antiangiogenic agents approved or undergoing clinical evaluation in RCC (46), and our evidence supports combining HC-5404 with any of these agents in the appropriate tumor context.

A previous report using the PERK inhibitor GSK2656157 revealed antiangiogenic effects as a single agent in BxPC3 pancreatic cancer xenografts (31), which was not observed with HC-5404 at the doses tested. In our findings, the antiangiogenic potential of HC-5404 was only uncovered when combined with stress-inducing VEGFR-TKI. Importantly, our studies used doses that were efficacious but did not induce pancreas effects reported with the GSK PERK inhibitor. It is possible that higher doses of HC-5404 could potentially have anti-vascular effects as a monotherapy. Instead, we demonstrate that the antitumor and antiangiogenic effects of HC-5404 can be potentiated by cotreatment with VEGFR-TKI while avoiding toxicity challenges associated with higher doses. While targeting PERK alone achieved moderate TGI of approximately 40% to 50% in responsive RCC models, enhancing tumor stress using antiangiogenic agents revealed a context-dependent therapeutic vulnerability that results in tumor regression. It is notable that the GSK series has off-target effects, including tyrosine kinases and RIPK1 (47), which may contribute to the activity of this compound and complicates a direct head-to-head comparison of the two PERK inhibitors. Treatments in our studies appeared to be well tolerated across all combinations, as no treatment-related body weight loss was observed. While observing no effect on mouse body weight was provisionally reassuring, future assessment will evaluate the tolerability of the combination treatments.

When the ability to mitigate ER stress is inhibited, chronic stress results in apoptosis through induction of the ATF4–CHOP axis (48). Blocking PERK likely exacerbates tumor stress, which was evidenced by elevated ATF4 pathway markers observed in HC-5404–treated groups. The induction of ASNS, CBS, CTH, and other downstream targets of ATF4 may be indicative of the accumulation of unresolved ER stress that occurs when PERK is inhibited in tumors. Similar findings were reported using the PERK inhibitor GSK2656157 (31), confirming this effect is likely target-mediated. Although ATF4 translation is typically induced by pPERK in response to ER stress, there are three other ISR kinases that activate ATF4 through phosphorylation of eIF2α(Ser51) (49). We have observed modest increases in peIF2α in response to HC-5404 *in vivo*, suggesting ISR pathway activation as a possible feedback response to PERK inhibition in tumors. Understanding this feedback mechanism and its role in tumor response is a focus of our ongoing research.

One of the early initiating factors of RCC is loss-of-function mutations in the *VHL* gene, which results in tumors that are highly vascularized and sensitive to antiangiogenic agents (33). Although initial data suggested that the combination benefit was exclusive to *VHL*-mutant cell-line models, an expanded follow-up study in RCC PDX revealed multiple VHL WT models that responded favorably and benefited from the combination treatment. The data at this time do not

support advancing VHL-mutant status as a clinical marker that would exclude patients from future combination clinical trials. However, given that a modest difference in sensitivity between *VHL*-mutant and *VHL*-WT PDX models was observed, there could still be potential to develop VHL status as a clinical biomarker. In the future, retrospective analyses of patients with RCC will evaluate the relationship between VHL mutation status and sensitivity to HC-5404/ VEGFR-TKI combinations.

The general applicability of HC-5404 to multiple VEGFR-TKI and the response observed across diverse tumor models highlights the clinical opportunity to improve patient outcomes by combining HC-5404 with standard-of-care VEGFR-TKI in RCC. VEGFR-TKI have been approved for multiple cancer types, including metastatic colorectal carcinoma (regorafenib; ref. 50), hepatocellular carcinoma (cabozantinib, sorafenib, lenvatinib, regorafenib; ref. 51), and thyroid cancers (cabozantinib, sorafenib, lenvatinib; ref. 52), among others. Given the widespread sensitivity to HC-5404/VEGFR-TKI combinations across diverse RCC PDX tumor models, it is possible that the mechanisms driving the interaction are conserved across cancer types. Future research is aimed at expansion of HC-5404/VEGFR-TKI combinations into any indication where antiangiogenic agents are approved for use in patients. Furthermore, VEGFR-TKI are currently used in combination with immune-checkpoint inhibitors as first-line therapies in advanced RCC, and recent publications highlight the stimulatory effect of PERK inhibition on the tumor immune microenvironment (53–55). Ongoing studies in syngeneic tumor models are evaluating the role of HC-5404 in promoting the antitumor activity of ICI/VEGFR-TKI combinations, with the goal of enhancing standard-of-care first-line therapies in RCC and beyond.

Authors' Disclosures

J. Gasparek reports other support from Curia during the conduct of the study. M. Betzenhauser reports other support from Curia Global during the conduct of the study and other support from Curia Global outside the submitted work. K.A. Staschke reports grants and personal fees from HiberCell, Inc. during the conduct of the study. No disclosures were reported by the other authors.

Authors' Contributions

M.E. Stokes: Conceptualization, formal analysis, supervision, validation, investigation, writing–original draft, project administration, writing–review and editing. **V. Calvo:** Conceptualization, formal analysis, supervision, investigation, writing–original draft, project administration. **S. Fujisawa:** Investigation, visualization, methodology, writing–review and editing. **C. Dudgeon:** Conceptualization, investigation, methodology, writing–original draft. **S. Huang:** Investigation, visualization, methodology. **N. Ballal:** Investigation. **L. Shen:** Investigation. **J. Gasparek:** Investigation. **M. Betzenhauser:** Supervision, investigation, methodology. **S.J. Taylor:** Formal analysis, investigation, writing–review and editing. **K.A. Staschke:** Supervision, investigation, writing–review and editing. **A.C. Rigby:** Conceptualization, resources, supervision, funding acquisition, investigation, writing–review and editing. **M.J. Mulvihill:** Resources, formal analysis, supervision, funding acquisition, project administration. **N. Bose:** Conceptualization, resources, supervision, funding acquisition, investigation, writing–review and editing. **E.S. Lightcap:** Supervision, funding acquisition, investigation, writing–review and editing. **D. Surguladze:** Conceptualization, resources, supervision, funding acquisition, methodology, writing–original draft, project administration, writing–review and editing.

Acknowledgments

We are grateful to Dr. Julio Aguirre-Ghiso for sharing the T-HEP3-PERK cell line and for providing new insights into the role of PERK in cancer stress biology and metastasis. We would also like to thank John Fuller for assistance with figure generation. All research funding was provided by HiberCell, Inc.

The publication costs of this article were defrayed in part by the payment of publication fees. Therefore, and solely to indicate this fact, this article is hereby marked "advertisement" in accordance with 18 USC section 1734.

Note

Supplementary data for this article are available at Clinical Cancer Research Online (http://clincancerres.aacrjournals.org/).

Received April 21, 2023; revised July 28, 2023; accepted September 19, 2023; published first September 21, 2023.

References

1. Haibe Y, Kreidieh M, El Hajj H, Khalifeh I, Mukherji D, Temraz S, et al. Resistance mechanisms to anti-angiogenic therapies in cancer. Front Oncol 2020;10:221.
2. Bergers G, Hanahan D. Modes of resistance to anti-angiogenic therapy. Nat Rev Cancer 2008;8:592–603.
3. Motzer RJ, Hutson TE, Tomczak P, Michaelson MD, Bukowski RM, Rixe O, et al. Sunitinib versus interferon alfa in metastatic renal-cell carcinoma. N Engl J Med 2007;356:115–24.
4. Escudier B, Eisen T, Stadler WM, Szczylik C, Oudard S, Siebels M, et al. Sorafenib in advanced clear-cell renal-cell carcinoma. N Engl J Med 2007;356:125–34.
5. Hu-Lowe DD, Zou HY, Grazzini ML, Hallin ME, Wickman GR, Amundson K, et al. Nonclinical antiangiogenesis and antitumor activities of axitinib (AG-013736), an oral, potent, and selective inhibitor of vascular endothelial growth factor receptor tyrosine kinases 1, 2, 3. Clin Cancer Res 2008;14:7272–83.
6. Rini BI, Escudier B, Tomczak P, Kaprin A, Szczylik C, Hutson TE, et al. Comparative effectiveness of axitinib versus sorafenib in advanced renal cell carcinoma (AXIS): a randomised phase 3 trial. Lancet North Am Ed 2011;378:1931–9.
7. Yamamoto Y, Matsui J, Matsushima T, Obaishi H, Miyazaki K, Nakamura K, et al. Lenvatinib, an angiogenesis inhibitor targeting VEGFR/FGFR, shows broad antitumor activity in human tumor xenograft models associated with microvessel density and pericyte coverage. Vasc Cell 2014;6:18.
8. Motzer RJ, Hutson TE, Glen H, Michaelson MD, Molina A, Eisen T, et al. Lenvatinib, everolimus, and the combination in patients with metastatic renal cell carcinoma: a randomised, phase 2, open-label, multicentre trial. Lancet Oncol 2015;16:1473–82.
9. Choueiri TK, Escudier B, Powles T, Tannir NM, Mainwaring PN, Rini BI, et al. Cabozantinib versus everolimus in advanced renal cell carcinoma (METEOR): final results from a randomised, open-label, phase 3 trial. Lancet Oncol 2016;17:917–27.
10. Yakes FM, Chen J, Tan J, Yamaguchi K, Shi Y, Yu P, et al. Cabozantinib (XL184), a novel MET and VEGFR2 inhibitor, simultaneously suppresses metastasis, angiogenesis, and tumor growth. Mol Cancer Ther 2011;10:2298–308.
11. Nakamura K, Taguchi E, Miura T, Yamamoto A, Takahashi K, Bichat F, et al. KRN951, a highly potent inhibitor of vascular endothelial growth factor receptor tyrosine kinases, has antitumor activities and affects functional vascular properties. Cancer Res 2006;66:9134–42.
12. Oudard S, Elaidi RT. Sequential therapy with targeted agents in patients with advanced renal cell carcinoma: optimizing patient benefit. Cancer Treat Rev 2012;38:981–7.
13. Tenold M, Ravi P, Kumar M, Bowman A, Hammers H, Choueiri TK, et al. Current approaches to the treatment of advanced or metastatic renal cell carcinoma. Am Soc Clin Oncol Educ Book 2020;40:1–10.
14. Han KS, Li N, Raven PA, Fazli L, Frees S, Ettinger S, et al. Inhibition of endoplasmic reticulum chaperone protein glucose-regulated protein 78 potentiates anti-angiogenic therapy in renal cell carcinoma through inactivation of the PERK/eIF2alpha pathway. Oncotarget 2015;6:34818–30.
15. Fels DR, Koumenis C. The PERK/eIF2alpha/ATF4 module of the UPR in hypoxia resistance and tumor growth. Cancer Biol Ther 2006;5:723–8.
16. Bi M, Naczki C, Koritzinsky M, Fels D, Blais J, Hu N, et al. ER stress-regulated translation increases tolerance to extreme hypoxia and promotes tumor growth. Embo J 2005;24:3470–81.

17. Kaufman RJ, Scheuner D, Schroder M, Shen X, Lee K, Liu CY, et al. The unfolded protein response in nutrient sensing and differentiation. Nat Rev Mol Cell Biol 2002;3:411–21.
18. Blais JD, Filipenko V, Bi M, Harding HP, Ron D, Koumenis C, et al. Activating transcription factor 4 is translationally regulated by hypoxic stress. Mol Cell Biol 2004;24:7469–82.
19. Wang Y, Alam GN, Ning Y, Visioli F, Dong Z, Nor JE, et al. The unfolded protein response induces the angiogenic switch in human tumor cells through the PERK/ATF4 pathway. Cancer Res 2012;72:5396–406.
20. Blais JD, Addison CL, Edge R, Falls T, Zhao H, Wary K, et al. Perk-dependent translational regulation promotes tumor cell adaptation and angiogenesis in response to hypoxic stress. Mol Cell Biol 2006;26:9517–32.
21. Makhov P, Naito S, Haifler M, Kutikov A, Boumber Y, Uzzo RG, et al. The convergent roles of NF-kappaB and ER stress in sunitinib-mediated expression of pro-tumorigenic cytokines and refractory phenotype in renal cell carcinoma. Cell Death Dis 2018;9:374.
22. Calvo V, Surguladze D, Li AH, Surman MD, Malibhatla S, Bandaru M, et al. Discovery of 2-amino-3-amido-5-aryl-pyridines as highly potent, orally bioavailable, and efficacious PERK kinase inhibitors. Bioorg Med Chem Lett 2021;43:128058.
23. Stokes ME, Surman MD, Calvo V, Surguladze D, Li AH, Gasparek J, et al. Optimization of a novel mandelamide-derived pyrrolopyrimidine series of PERK inhibitors. Pharmaceutics 2022;14:2233.
24. Fabian MA, Biggs WH 3rd, Treiber DK, Atteridge CE, Azimioara MD, Benedetti MG, et al. A small molecule-kinase interaction map for clinical kinase inhibitors. Nat Biotechnol 2005;23:329–36.
25. Tenkerian C, Krishnamoorthy J, Mounir Z, Kazimierczak U, Khoutorsky A, Staschke KA, et al. mTORC2 balances AKT activation and eIF2alpha serine 51 phosphorylation to promote survival under stress. Molecular cancer research : MCR 2015;13:1377–88.
26. Pakos-Zebrucka K, Koryga I, Mnich K, Ljujic M, Samali A, Gorman AM. The integrated stress response. EMBO Rep 2016;17:1374–95.
27. Chevet E, Hetz C, Samali A. Endoplasmic reticulum stress-activated cell reprogramming in oncogenesis. Cancer Discov 2015;5:586–97.
28. Costa-Mattioli M, Walter P. The integrated stress response: from mechanism to disease. Science 2020;368:eaat5314.
29. Tameire F, Verginadis II, Leli NM, Polte C, Conn CS, Ojha R, et al. ATF4 couples MYC-dependent translational activity to bioenergetic demands during tumour progression. Nat Cell Biol 2019;21:889–99.
30. Pytel D, Gao Y, Mackiewicz K, Katlinskaya YV, Staschke KA, Paredes MC, et al. PERK is a haploinsufficient tumor suppressor: gene dose determines tumor-suppressive versus tumor promoting properties of PERK in melanoma. PLos Genet 2016;12:e1006518.
31. Atkins C, Liu Q, Minthorn E, Zhang SY, Figueroa DJ, Moss K, et al. Characterization of a novel PERK kinase inhibitor with antitumor and antiangiogenic activity. Cancer Res 2013;73:1993–2002.
32. Kuo CY, Lin CH, Hsu T. VHL inactivation in precancerous kidney cells induces an inflammatory response via ER stress-activated IRE1alpha signaling. Cancer Res 2017;77:3406–16.
33. Baldewijns MM, van Vlodrop IJ, Vermeulen PB, Soetekouw PM, van Engeland M, de Bruine AP. VHL and HIF signalling in renal cell carcinogenesis. J Pathol 2010;221:125–38.
34. Zhu J, Berisa M, Schworer S, Qin W, Cross JR, Thompson CB. Transsulfuration activity can support cell growth upon extracellular cysteine limitation. Cell Metab 2019;30:865–76.
35. Brodaczewska KK, Szczylik C, Fiedorowicz M, Porta C, Czarnecka AM. Choosing the right cell line for renal cell cancer research. Mol Cancer 2016;15:83.
36. Izumchenko E, Paz K, Ciznadija D, Sloma I, Katz A, Vasquez-Dunddel D, et al. Patient-derived xenografts effectively capture responses to oncology therapy in a heterogeneous cohort of patients with solid tumors. Ann Oncol 2017;28:2595–605.
37. Hidalgo M, Bruckheimer E, Rajeshkumar NV, Garrido-Laguna I, De Oliveira E, Rubio-Viqueira B, et al. A pilot clinical study of treatment guided by personalized tumorgrafts in patients with advanced cancer. Mol Cancer Ther 2011;10:1311–6.
38. Falcon BL, Chintharlapalli S, Uhlik MT, Pytowski B. Antagonist antibodies to vascular endothelial growth factor receptor 2 (VEGFR-2) as anti-angiogenic agents. Pharmacol Ther 2016;164:204–25.
39. Kruger-Genge A, Blocki A, Franke RP, Jung F. Vascular endothelial cell biology: an update. International journal of molecular sciences. 2019;20:4411.
40. Ellis LM, Hicklin DJ. VEGF-targeted therapy: mechanisms of anti-tumour activity. Nat Rev Cancer 2008;8:579–91.
41. Yamazaki T, Mukouyama YS. Tissue specific origin, development, and pathological perspectives of pericytes. Front Cardiovasc Med 2018;5:78.
42. Guerin E, Man S, Xu P, Kerbel RS. A model of postsurgical advanced metastatic breast cancer more accurately replicates the clinical efficacy of antiangiogenic drugs. Cancer Res 2013;73:2743–8.
43. Bridgeman VL, Vermeulen PB, Foo S, Bilecz A, Daley F, Kostaras E, et al. Vessel co-option is common in human lung metastases and mediates resistance to anti-angiogenic therapy in preclinical lung metastasis models. J Pathol 2017;241:362–74.
44. Frentzas S, Simoneau E, Bridgeman VL, Vermeulen PB, Foo S, Kostaras E, et al. Vessel co-option mediates resistance to anti-angiogenic therapy in liver metastases. Nat Med 2016;22:1294–302.
45. Cuypers A, Truong AK, Becker LM, Saavedra-Garcia P, Carmeliet P. Tumor vessel co-option: the past & the future. Front Oncol 2022;12:965277.
46. Vachhani P, George S. VEGF inhibitors in renal cell carcinoma. Clin Adv Hematol Oncol 2016;14:1016–28.
47. Rojas-Rivera D, Delvaeye T, Roelandt R, Nerinckx W, Augustyns K, Vandenabeele P, et al. When PERK inhibitors turn out to be new potent RIPK1 inhibitors: critical issues on the specificity and use of GSK2606414 and GSK2656157. Cell Death Differ 2017;24:1100–10.
48. Iurlaro R, Munoz-Pinedo C. Cell death induced by endoplasmic reticulum stress. FEBS J 2016;283:2640–52.
49. Wang X, Proud CG. The role of eIF2 phosphorylation in cell and organismal physiology: new roles for well-known actors. Biochem J 2022;479:1059–82.
50. Xie YH, Chen YX, Fang JY. Comprehensive review of targeted therapy for colorectal cancer. Signal Transduct Target Ther 2020;5:22.
51. Mou L, Tian X, Zhou B, Zhan Y, Chen J, Lu Y, et al. Improving outcomes of tyrosine kinase inhibitors in hepatocellular carcinoma: new data and ongoing trials. Front Oncol 2021;11:752725.
52. Puliafito I, Esposito F, Prestifilippo A, Marchisotta S, Sciacca D, Vitale MP, et al. Target therapy in thyroid cancer: current challenge in clinical use of tyrosine kinase inhibitors and management of side effects. Front Endocrinol (Lausanne) 2022;13:860671.
53. Hurst KE, Lawrence KA, Essman MT, Walton ZJ, Leddy LR, Thaxton JE. Endoplasmic reticulum stress contributes to mitochondrial exhaustion of CD8(+) T cells. Cancer Immunol Res 2019;7:476–86.
54. Raines LN, Zhao H, Wang Y, Chen HY, Gallart-Ayala H, Hsueh PC, et al. PERK is a critical metabolic hub for immunosuppressive function in macrophages. Nat Immunol 2022;23:431–45.
55. Mandula JK, Chang S, Mohamed E, Jimenez R, Sierra-Mondragon RA, Chang DC, et al. Ablation of the endoplasmic reticulum stress kinase PERK induces paraptosis and type I interferon to promote anti-tumor T cell responses. Cancer Cell 2022;40:1145–60.